Effect of Nucleic Acid Binding on the Triplet State Properties of Tetrapeptides Containing Tryptophan and 6-Methyltryptophan: A Study by Phosphorescence and ODMR Spectroscopy†

Ajay Misra,‡ Andrzej Ozarowski,‡ Jose R. Casas-Finet,§ and August H. Maki*,‡

Department of Chemistry, University of California, Davis, California 95616, and AIDS Vaccine Program, SAIC Frederick, National Cancer Institute−Frederick Cancer Research and Development Center, Frederick, Maryland 21702-1201

Received July 6, 2000; Revised Manuscript Received September 13, 2000

ABSTRACT: Complexes of four peptides [KWGK, KGWK, K(6MeW)GK, KG(6MeW)K] with the nucleic acids [poly(A), poly(C), poly(U), poly(I), and rG_8] have been investigated by phosphorescence and optically detected magnetic resonance (ODMR) spectroscopy. The intrinsic spectroscopic probes used in these studies are tryptophan (W) and 6-methyltryptophan (6MeW). Binding to the nucleic acids results in a red-shift of the phosphorescence 0,0-band ($\Delta E_{0,0}$) of the aromatic residue as well as a reduction of its zero-field splitting parameter (ΔD). Results are compared with earlier studies of the HIV-1 nucleocapsid protein, NCp7, that contains a single tryptophan residue (Trp37) within a retroviral zinc finger sequence. Binding of poly(A) or poly(U) to the tetrapeptides induces larger $\Delta E_{0,0}$ and ΔD than when bound to NCp7, indicating stronger stacking interactions. Poly(I), on the other hand, produces larger shifts in Trp37 of NCp7. Binding of rG_8 produces sequence-dependent effects in the peptides. When bound to NCp7, but in contrast with tetrapeptide binding, nucleic acids produce large changes in triplet state kinetics consistent with enhanced spin−orbit coupling. These results are discussed in terms of three limiting types of tryptophan−base interaction: intercalation, aromatic stacking, and edge-on interaction. These should have differing effects on the properties of the triplet state.

Interactions between proteins and nucleic acids play a vital role in the functioning of biological systems, e.g., gene regulation, DNA replication, recombination, repair, and transcription. Many DNA binding proteins show sequence specificity in their binding to duplex DNA. On the other hand, there are also numerous proteins involved in DNA and RNA metabolism that bind preferentially to single-stranded nucleic acids. Hence the binding specificity of proteins and nucleic acids depends at least partially on nucleic acid conformation. To understand the nature of protein−nucleic acid binding specificity, it is necessary to know not only the nucleic acid site to which the proteins binds but also the peptide sequence involved in the binding interface. These interactions generally involve electrostatic forces between phosphate anions of DNA or RNA and cationic amino acid side chains, hydrogen bonding interactions, hydrophobic contacts, and London dispersion forces that arise from the stacking of aromatic side chains and nucleic acid bases (*1*, *2*). Exposed aromatic side chains of tryptophan, tyrosine, and phenylalanine can contribute to the selective recognition of base sequences through stacking interactions involving π-electron overlap. These contributions could be of particular significance in peptide interactions with single-stranded RNA and DNA sequences. Quenching of tryptophan fluorescence, associated with and attributed to aromatic stacking interactions, has been observed in tryptophan−nucleoside aggregates formed in frozen aqueous solutions (*3*−*5*) and from complex formation by indole derivatives and small tryptophan-containing peptides such as lysyltryptophanyllysine with DNA and with various RNAs (*6*−*9*). Spectroscopic methods also have been used to study stacking interactions in covalently linked indole−base dimer models (*10*), in t-RNA synthetase complexes (*11*−*13*), and in complexes between DNA and T4 phage gene 32 protein (*14*). Specific effects of base stacking with the aromatic amino acids of peptides on the circular dichroism of poly(rA) and other helical polyribonucleotides has been reported (*15*), as well as ^{1}H NMR shifts attributed to stacking-induced ring current shifts in these systems (*16*−*18*). Extensive studies of aromatic stacking interactions of various tryptophan-containing peptides and proteins with DNA and RNA have been carried out using phosphorescence and optically detected magnetic resonance (ODMR)[1] spectroscopy (*19*−*25*). Studies of the binding thermodynamics of a series of oligolysines containing one, two, or three tryptophan residues to several single-stranded polynucleotides have been reported by Mascotti and Lohman (*26*, *27*).

In this paper, we report on the interaction of four tetrapeptides, each containing an aromatic amino acid, with a set of nucleic acids. Phosphorescence and ODMR measurements are reported on the complexes of lysyltryptopha-

† This publication was made possible by Grant ES-02662 from the National Institute of Environmental Health Sciences (A.H.M.) and by National Cancer Institute Contract N01-56000 (J.R.C.). Its contents are solely the responsibility of the authors and do not necessarily reflect the views of the NIEHS or NCI, NIH.

* To whom correspondence should be addressed: Phone: (530)-752-6471. Fax: (530)752-8995. E-mail: maki@indigo.ucdavis.edu.

‡ University of California.

§ National Cancer Institute−Frederick Cancer Research and Development Center.

10.1021/bi0015663 CCC: $19.00
Published on Web 10/21/2000

nylglycyllysine (KWGK), lysylglycyltryptophanyllysine (KGWK), and their 6-methyltryptophan analogues, K(6MeW)-GK and KG(6MeW)K with poly(A), poly(C), poly(U), poly-(I), and rG_8. We focus on the effects of nucleic acid binding on the triplet state properties of the aromatic amino acid. In previous work (*28*−*30*), we have shown that the triplet state energy and zero-field splitting (ZFS) parameters of tryptophan are sensitive to environmental perturbations. The four tetrapeptides studied here comprise two differing sequences and two related aromatic amino acids.

The purpose of this study is an attempt to discover differences in binding modes of altered peptide sequences to oligo- and polyribonucleotide models and to determine whether phosphorescence and ODMR spectroscopy can be used to detect and characterize these differences. This work is an offshoot of our continuing investigation of nucleic acid complexes of NCp7, the nucleocapsid protein of type 1 human immunodeficiency virus (HIV-1) and factors that determine its specific recognition of genomic RNA (*24*, *31*, *32*). The tetrapeptide sequences in this study are related to the sequence that flanks the single tryptophan residue of NCp7, located at position 37 in the C-terminal zinc finger motif of the 55 amino acid protein, ...KGCW^{37}KC..., where the cysteine residues are coordinated with zinc. The zinc finger sequences, the hydrophobic residues and the zinc-binding residues in particular, are required for accurate recognition and efficient packaging of HIV-1 genomic RNA (*33*, *34*). We have chosen these model tetrapeptides (KWGK and KGWK) to study differences between NCp7 and short tryptophan-containing peptides in their interactions with oligo- and polyribonucleotides and also to investigate why nature might have selected one sequence (KGWK) rather than, for instance, the related (KWGK) as the flanking sequence of Trp37 in NCp7. In addition, to study effects of amino acid modification on sequence dependence of the interactions we have studied an analogous pair of tetrapeptides differing only in the probe, i.e., 6-methyltryptophan vs tryptophan.

The shift of the ZFS parameter, *D*, and of the phosphorescence wavelength of tryptophan upon complex formation can be used to gauge the extent of π-electron interactions. Aromatic stacking interactions lead, in general, to a red-shift of the well-resolved phosphorescence 0,0-band of tryptophan and to a reduced value of *D* (*32*). The ZFS parameters, *D* and *E*, depend on the relative distribution of the triplet electron pair according to (*35*):

$$D = 3/4(\gamma\hbar)^2\langle(r_{12}^2 - 3z_{12}^2)/r_{12}^5\rangle_{av} \quad (1)$$

and

$$E = 3/4(\gamma\hbar)^2\langle(y_{12}^2 - x_{12}^2)/r_{12}^5\rangle_{av} \quad (2)$$

The spatial operators are averaged over the triplet state wave function, γ is the electron magnetogyric ratio, and $\hbar$ is Planck's constant over 2π. The ZFS parameters effectively scale as r_{12}^{-3}, making them extremely sensitive to the interelectron distance. *D* is positive for $^3(\pi,\pi^*)$ states of aromatic molecules such as tryptophan (*z* is normal to the aromatic plane), so its size is particularly sensitive to delocalization of the electron pair distribution along *z*, the stacking direction. It has been determined (*36*−*38*) that the solvent-induced phosphorescence red-shift of an aromatic triplet state is linearly correlated with a reduction of *D*. The proposed mechanism for this effect involves the solvent-induced mixing of higher energy *localized* triplet states that are more diffuse than the zero-order phosphorescent state. When aromatic stacking interactions induce *delocalized* charge-transfer character into the phosphorescent state, reduction of the *D* value is expected to be particularly large (*39*).

MATERIALS AND METHODS

The tetrapeptides were synthesized by Macromolecular Resources (Fort Collins, CO), purified to better than 90% by reverse-phase HPLC, and assessed by MALDI mass spectroscopy. Fmoc 6-methyltryptophan precursor was prepared by Peptide Technologies (Gaithersburg, MD), purified by HPLC, and assessed by elemental analysis and electrospray MS. The tryptophan-containing peptides contained all L-enantiomers, whereas the 6-methyltryptophan peptides were L- but they contained both D- and L-6-methyltryptophan. Poly(U), poly(C), poly(A), and poly(I) were lyophilized samples purchased from Pharmacia. rG_8 was prepared by Macromolecular Resources and purified by HPLC. Peptides and nucleic acids were dissolved in deionized doubly distilled water. Complexes were formed by adding an aliquot of peptide solution to nucleic acid solution and mixing for 1 h. Ethylene glycol was added as cryosolvent to 40% v/v. The final peptide concentration was ca. 0.4 mM, and nucleotide monomer was in 10-fold excess. Samples, ca. 50 μL, were introduced into 2 mm i.d. Spectrasil tubes for phosphorescence and ODMR measurements.

Phosphorescence measurements were made at 77 and 4.2 K using excitation by a 100-W high-pressure Hg arc lamp whose output was filtered through a monochromator (16 nm band-pass). The phosphorescence/ODMR spectrometer, using photon counting, has been described elsewhere (*40*, *41*). ODMR experiments were carried out in the absence of an applied magnetic field at the temperature of pumped liquid He, 1.2 K in our apparatus, to minimize spin lattice relaxation (SLR).

The delayed slow-passage ODMR experiments and their analysis to obtain ν_0 and $\nu_{1/2}$, the band center frequency and its half-width at half-maximum, respectively, have been described recently (*42*, *43*). Signal accumulation is started after a delay, t_0, following cessation of optical pumping. After an additional delay of 2−3 s, to accumulate baseline data, the microwave sweep is begun. The sublevel decay and the SLR rate constants obtained from global analysis of microwave-induced delayed phosphorescence (MIDP) responses (see below) were used for fitting the delayed ODMR signal. In most cases only two of the ODMR bands (*D*−*E*, 2*E*) of tryptophan or 6-methyltryptophan could be obtained with adequate signal/noise; the ZFS parameters, *D* and *E*, were

[1] Abbreviations: A, adenine; C, cysteine or cytosine; 6MeW, 6-methyltryptophan; CT, charge transfer; *D* and *E*, zero-field splitting parameters; EA, electron affinity; Fmoc, N-(9-fluorenylmethoxy)-carbonyl derivative; G, glycine or guanine; I, inosine; IP, ionization potential; ISC, intersystem crossing; K, lysine; MIDP, microwave-induced delayed phosphorescence; NCp7, nucleocapsid protein of human immunodeficiency virus, type 1; ODMR, optically detected magnetic resonance; SLR, spin−lattice relaxation; SOC, spin−orbit coupling; U, uracil; W, tryptophan; ZFS, zero-field splittings.

Table 1: Triplet State Spectroscopic Properties of KWGK, KGWK, and Their Complexes with Nucleic Acids[a]

		$D-E$		$2E$				
sample	$\lambda_{0,0}$ (nm)[b]	ν_0 (GHz)	$\nu_{1/2}$ (MHz)	ν_0 (GHz)	$\nu_{1/2}$ (MHz)	D (GHz)	E (GHz)	$10^6\Delta D/\Delta E_{0,0}$
KWGK	407.5	1.750 (1)	63 (1)	2.520 (6)	122 (10)	3.011	1.260	
KWGK + poly(C)		1.728 (2)	74 (5)	2.529 (4)	125 (6)	2.993	1.264	
KWGK + rG_8	410.1	1.705 (7)	70 (6)	2.51 (1)	118 (13)	2.96	1.26	11 (2)
KWGK + poly(A)	411.2	1.687 (1)	70 (3)	2.490 (2)	120 (9)	2.934	1.246	12 (1)
KWGK + poly(I)	412.4	1.673 (2)	76 (1)	2.50 (1)	166 (15)	2.92	1.25	10 (2)
KWGK + poly(U)	413.2	1.665 (3)	92 (3)	2.526 (4)	200 (37)	2.928	1.263	8 (1)
KGWK	408.8	1.735 (1)	66 (1)	2.523 (3)	131 (9)	2.997	1.261	
KGWK + poly(C)		1.723 (4)	73 (3)	2.528 (6)	129 (9)	2.987	1.264	
KGWK + rG_8	410.8	1.708 (2)	77 (3)	2.543 (9)	155 (10)	2.979	1.271	5 (2)
KGWK + poly(A)	410.8	1.681 (9)	80 (9)	2.54 (1)	234 (5)	2.95	1.26	13 (3)
KGWK + poly(I)	411.8	1.679 (2)	73 (2)	2.538 (7)	150 (10)	2.948	1.269	9 (1)
KGWK + poly(U)	413.1	1.658 (3)	84 (4)	2.520 (5)	172 (10)	2.918	1.26	10 (1)

[a] Standard deviations in the last digit are given in parentheses. [b] 0,0 band of W, excitation at 297 nm.

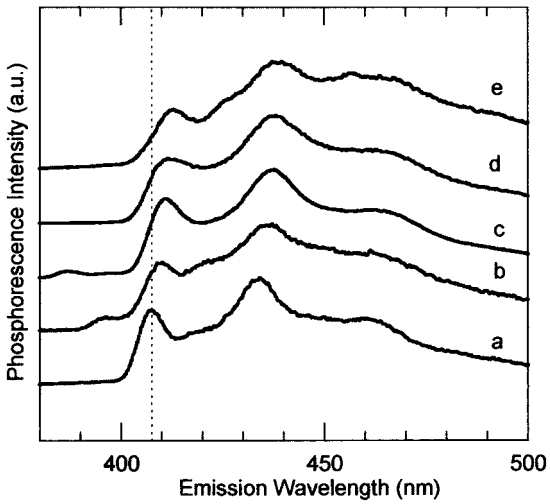

FIGURE 1: Phosphorescence spectra of (a) KWGK, (b) KWGK + rG_8, (c) KWGK + poly(A), (d) KWGK + poly(I), and (e) KWGK + poly(U) in ethylene glycol−water glass at 4 K. Samples are excited at 297 nm with 16 nm bandwidth and observed at 3.2 nm resolution.

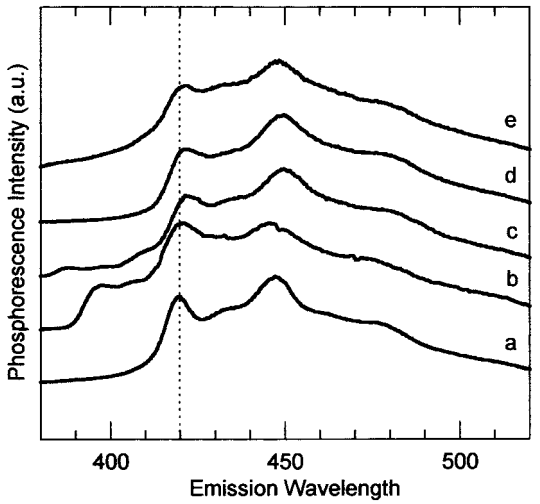

FIGURE 2: Phosphorescence spectra of (a) K(6MeW)GK, (b) K(6MeW)GK + rG_8, (c) K(6MeW)GK + poly(A), (d) K(6MeW)-GK + poly(I), and (e) K(6MeW)GK + poly(U) in ethylene glycol−water glass at 4 K. Samples are excited at 302 nm with 16 nm bandwidth and observed at 3.2 nm resolution.

obtained from the following expressions:

$$D = [(1/2)\nu_0(2E) + \nu_0(D-E)] \quad (3)$$

$$E = (1/2)\nu_0(2E) \quad (4)$$

To obtain the sublevel decay rate constants k_x, k_y, and k_z, we employed global analysis of MIDP data sets (*40*), which typically involve the least-squares fittings of ca. 20 000 data points. If two or all three of the transitions are analyzed globally, both the decay rate constants and the SLR rate constants can be determined. Global MIDP analysis also was used to obtain relative sublevel radiative rate constants and populating rates.

EXPERIMENTAL RESULTS

Phosphorescence Spectra. The phosphorescence spectra of KWGK and its nucleic acid complexes are shown in Figure 1. The 0,0-band of tryptophan is shifted to the red, and the spectrum is somewhat broadened in the complexes. A weak component from the nucleic acids is present in the spectra of the poly(A) and rG_8 complexes, but it was not intense enough to prevent measurement of the tryptophan 0,0-band wavelength. Similar spectra are exhibited by KGWK. All spectra display the characteristic vibronic bands of tryptophan. The peak 0,0-band wavelengths for these peptides are listed in Table 1. The spectrum of K(6MeW)-GK and its nucleic acid complexes are shown in Figure 2. The complexes reveal a red-shift relative to the free peptide. The spectra show well-resolved vibronic structure similar to that of tryptophan, but the 0,0-band is shifted to the red of KWGK by ca. 12 nm. The phosphorescence of K(6MeW)-GK resembles that of free 6-methyltryptophan, except that its 0,0-band is shifted about 2 nm to the red of the free amino acid (*44*), suggesting a more polarizable microenvironment in the peptide (*45*). The 0,0-band peak wavelengths of the 6-methyltryptophan tetrapeptides and their nucleic acid complexes are listed in Table 2. A red-shift of the 0,0-band peak is apparent in the spectra of those complexes whose phosphorescence was dominated by the amino acid. The complex of K(6MeW)GK with rG_8 was dominated by intense G background (Figure 2, spectrum b), so the 6-methyltryptophan 0,0-band wavelength could not be determined. Each poly(C) complex was dominated by a broad emission from cytosine preventing the accurate measurement of the tryptophan or 6-methyltryptophan 0,0-bands.

Table 2: Triplet State Spectroscopic Properties of K(6MeW)GK, KG(6MeW)K, and Their Complexes with Nucleic Acids[a]

		$\|D\|-\|E\|$		$2\|E\|$				
sample	$\lambda_{0,0}$ (nm)[b]	ν_0 (GHz)	$\nu_{1/2}$ (MHz)	ν_0 (GHz)	$\nu_{1/2}$ (MHz)	$\|D\|$ (GHz)	$\|E\|$ (GHz)	$10^6\Delta D/\Delta E_{0,0}$
K(6MeW)GK	419.7	1.5943 (8)	50 (6)	2.640 (6)	100 (5)	2.914	1.320	
K(6MeW)GK + poly(C)		1.577 (3)	56 (9)	2.619 (1)	108 (7)	2.887	1.309	
K(6MeW)GK + rG_8		1.569 (4)	73 (12)	2.523 (4)	48 (2)	2.831	1.261	
K(6MeW)GK + poly(A)	423.5	1.548 (7)	62 (3)	2.604 (2)	123 (9)	2.850	1.302	10 (1)
K(6MeW)GK + poly(I)	421.8	1.565 (3)	66 (1)	2.621 (1)	120 (10)	2.875	1.310	11 (1)
K(6MeW)GK + poly(U)	421.5	1.573 (5)	80 (10)	2.63 (1)	114 (8)	2.89	1.32	8 (2)
KG(6MeW)K	420.5	1.579 (2)	51.4 (8)	2.670 (2)	92 (1)	2.912	1.335	
KG(6MeW)K + poly(C)	421.2	1.568 (4)	61 (9)	2.66 (1)	74 (19)	2.90	1.33	
KG(6MeW)K + rG_8	423.1	1.555 (5)	59 (8)	2.672 (7)	102 (18)	2.891	1.336	5 (1)
KG(6MeW)K + poly(A)	423.5	1.543 (7)	51 (1)	2.645 (1)	114 (10)	2.865	1.322	9 (1)
KG(6MeW)K + poly(I)	424.1	1.541 (2)	63 (2)	2.644 (5)	118 (2)	2.863	1.321	8 (1)
KG(6MeW)K + poly(U)	423.9	1.5254 (2)	69 (4)	2.666 (8)	111 (15)	2.858	1.333	9 (1)

[a] Standard deviations in the last digit are given in parentheses. [b] 0,0 band of 6MeW, excitation at 302 nm.

Table 3: Kinetic and Radiative Parameters of KWGK, KGWK, and Their Complexes with Nucleic Acids[a]

sample[b]	k_x (s^{-1})	k_y (s^{-1})	k_z (s^{-1})	R_{zx}[c]	R_{yx}[c]	w_{xy} (s^{-1})[d]	w_{xz} (s^{-1})[d]	w_{yz} (s^{-1})[d]	p_x[e]	p_y[e]	p_z[e]
KWGK	0.341 (7)	0.107 (4)	0.000 (2)	0.001 (9)	0.075 (8)	0.009 (2)	0.027 (4)	0.0467 (5)	0.36	0.61	0.03
KWGK + poly(C)	0.39 (2)	0.13 (1)	0.00 (1)	0.00 (2)	0.10 (2)	0.000 (8)	0.02 (1)	0.049 (2)	0.33	0.47	0.20
KWGK + rG_8	0.41 (6)	0.12 (4)	0.00 (2)	0.00 (6)	0.10 (6)	0.01 (2)	0.03 (3)	0.044 (4)	0.41	0.41	0.18
KWGK + poly(A)	0.36 (1)	0.104 (5)	0.000 (3)	0.00 (1)	0.075 (9)	0.017 (4)	0.035 (5)	0.040 (5)	0.31	0.56	0.13
KWGK + poly(I)	0.395 (8)	0.117 (4)	0.006 (3)	0.019 (8)	0.065 (8)	0.017 (3)	0.020 (4)	0.0407 (5)	0.41	0.48	0.11
KWGK + poly(U)	0.41 (1)	0.108 (9)	0.000 (6)	0.00 (1)	0.03 (1)	0.046 (6)	0.030 (8)	0.037 (1)	0.54	0.33	0.12
KGWK	0.351 (9)	0.106 (4)	0.004)	0.000 (9)	0.098 (8)	0.011 (3)	0.034 (4)	0.0372 (4)	0.43	0.48	0.09
KGWK + poly(C)	0.37 (1)	0.12 (1)	0.000 (7)	0.00 (2)	0.09 (2)	0.010 (7)	0.02 (1)	0.045 (1)	0.31	0.47	0.22
KGWK + rG_8	0.36 (3)	0.11 (1)	0.000 (9)	0.00 (3)	0.04 (2)	0.03 (2)	0.03 (2)	0.046 (1)	0.36	0.47	0.17
KGWK + poly(A)	0.35 (1)	0.113 (6)	0.002 (3)	0.00 (1)	0.00 (1)	0.047 (4)	0.033 (5)	0.0482 (7)	0.37	0.50	0.13
KGWK + poly(I)	0.38 (1)	0.105 (4)	0.000 (2)	0.000 (8)	0.058 (7)	0.041 (4)	0.036 (5)	0.0491 (6)	0.41	0.48	0.11
KGWK + poly(U)	0.39 (1)	0.112 (7)	0.000 (5)	0.00 (1)	0.04 (1)	0.040 (5)	0.028 (7)	0.0402 (9)	0.46	0.39	0.14

[a] Standard deviations in the last digit are given in parentheses. [b] Excitation at 297 nm except as noted. [c] R_{ix} is the radiative rate constant of T_i relative to T_x. [d] w_{ij} is the $T_i \leftrightarrow T_j$ spin−lattice relaxation rate constant. [e] Corrected values, see text. Estimated errors in the p_i are ±0.03.

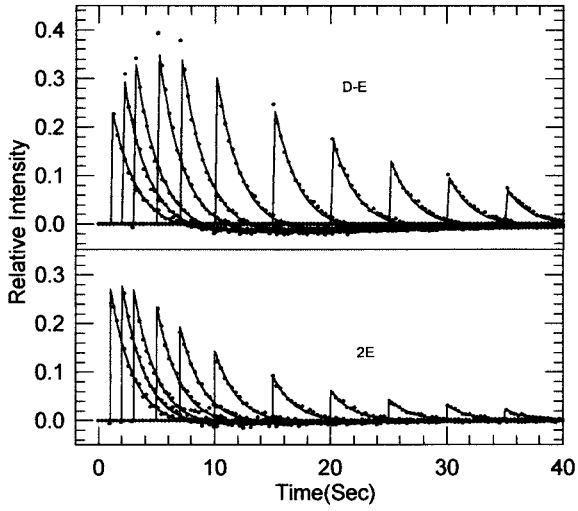

FIGURE 3: MIDP responses of tryptophan in the KWGK complexed with poly(I) at various delay times for the $D-E$ transition (top) and for the $2E$ transition (bottom). Superimposed on the data points are the MIDP responses calculated by global analysis using the best-fit kinetic parameters listed in Table 3.

Microwave-Induced Delayed Phosphorescence. A set of MIDP data for the $D-E$ and $2E$ microwave transition of tryptophan in the complex of KWGK with poly(I) is shown in Figure 3. The sublevel decay constants (k_i), SLR rate constants (w_{ij}), and relative radiative rate constants (k_i^r), ($i, j = x, y, z$) of each peptide and its complexes obtained from global analysis (*40*) are listed in Tables 3 and 4.

The k_i and w_{ij} can be used to form the rate constant matrix, **R**, from which one can obtain the sublevel populating vector, **p**, by solving

$$\mathbf{p} - \mathbf{R} \times \mathbf{n^0} = \mathbf{0} \tag{5}$$

where $\mathbf{n^0}$ is the vector of steady-state populations and **0** is the null vector (*40*). If the duration of optical pumping is sufficiently long, the initial populations at the beginning of the MIDP measurement may be used as the elements of $\mathbf{n^0}$; best-fit values for the initial populations result from the global least-squares analysis. Thus, **p** can be obtained by solving eq 5. Since only the relative values of the $\mathbf{n^0}$ elements are introduced, the elements of **p** obtained from eq 5 are relative as well. The samples were optically pumped for 15 s in our measurements. Thus, the initial population of T_x is a reasonable approximation for n_x^0, but n_z^0 and to a lesser extent n_y^0 will be underestimated, and the values of p_z and p_y obtained from MIDP using eq 5 will be too low. We have employed a new kinetic method, global analysis of microwave-induced phosphorescence transients obtained during the optical pumping cycle (*46*) to obtain relative values of p_i that are not subject to this error. The elements of **p** for the peptides and their nucleic acid complexes that are listed in Tables 3 and 4 have been corrected for the deviations from steady-state populations that occur in our measurements.

Delayed Slow Passage ODMR. The delayed slow-passage ODMR spectra of the $D-E$ transition of tryptophan in the peptide KWGK and its complex with poly(U) are shown in Figure 4. The superimposed solid lines are least-squares fittings yielding the ν_0 and $\nu_{1/2}$ values that are given in Table 1. Examples of delayed slow passage spectra of the $2E$

Table 4: Kinetic and Radiative Parameters of K(6MeW)GK, KG(6MeW)K, and Their Complexes with Nucleic Acids[a]

sample[b]	k_x (s^{-1})	k_y (s^{-1})	k_z (s^{-1})	R_{zx}[c]	R_{yx}[c]	w_{xy} (s^{-1})[d]	w_{xz} (s^{-1})[d]	w_{yz} (s^{-1})[d]	p_x[e]	p_y[e]	p_z[e]
K(6MeW)GK	0.37 (2)	0.11 (1)	0.01 (1)	0.02 (2)	0.10 (2)	0.000 (8)	0.01 (1)	0.038 (1)	0.38	0.53	0.09
K(6MeW)GK + poly(C)	0.366 (5)	0.123 (5)	0.009 (3)	0.000 (3)	0.075 (3)	0.000 (3)	0.018 (3)	0.037 (3)	0.25	0.52	0.23
K(6MeW)GK + rG_8	0.47 (2)	0.15 (1)	0.00 (3)	0.00 (3)	0.09 (1)	0.000 (3)	0.0190 (8)	0.0475 (8)	0.41	0.40	0.19
K(6MeW)GK + poly(A)	0.42 (1)	0.13 (1)	0.001 (6)	0.01 (1)	0.11 (1)	0.001 (6)	0.025 (9)	0.048 (1)	0.39	0.55	0.06
K(6MeW)GK + poly(I)	0.40 (3)	0.11 (1)	0.00 (1)	0.00 (2)	0.07 (2)	0.02 (1)	0.03 (1)	0.051 (2)	0.40	0.53	0.07
K(6MeW)GK + poly(U)	0.42 (1)	0.12 (3)	0.00 (2)	0.00 (6)	0.12 (5)	0.01 (2)	0.02 (3)	0.046 (3)	0.45	0.41	0.14
KG(6MeW)K	0.332 (8)	0.108 (4)	0.000 (2)	0.000 (7)	0.046 (6)	0.041 (2)	0.0350 (4)	0.0492 (5)	0.36	0.56	0.08
KG(6MeW)K + poly(C)	0.43 (3)	0.12 (2)	0.00 (1)	0.00 (3)	0.08 (2)	0.00 (1)	0.02 (2)	0.035 (2)	0.27	0.47	0.26
KG(6MeW)K + rG_8	0.40 (3)	0.11 (1)	0.00 (1)	0.00 (3)	0.08 (2)	0.02 (1)	0.03 (1)	0.044 (1)	0.45	0.42	0.13
KG(6MeW)K + poly(A)	0.37 (1)	0.117 (8)	0.000 (5)	0.00 (1)	0.07 (1)	0.019 (5)	0.033 (8)	0.0445 (9)	0.32	0.59	0.09
KG(6MeW)K + poly(I)	0.37 (1)	0.100 (4)	0.000 (2)	0.000 (8)	0.030 (7)	0.052 (4)	0.036 (5)	0.0467 (7)	0.35	0.54	0.11
KG(6MeW)K + poly(U)	0.42 (1)	0.101 (7)	0.004 (5)	0.00 (1)	0.06 (1)	0.029 (5)	0.028 (7)	0.0322 (8)	0.43	0.39	0.18

[a] Standard deviations in the last digit are given in parentheses. [b] Excitation at 302 nm except as noted. [c] R_{ix} is the radiative rate constant of T_i relative to T_x. [d] w_{ij} is the $T_i \leftrightarrow T_j$ spin−lattice relaxation rate constant. [e] Corrected values, see text. Estimated errors in the p_i are ±0.03.

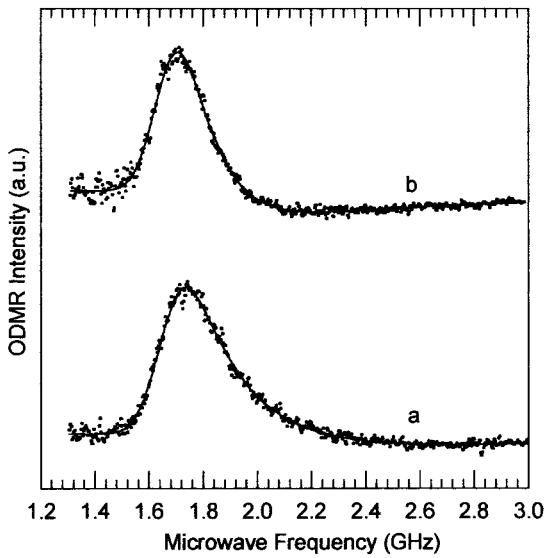

FIGURE 4: Delayed slow-passage ODMR spectra of $D-E$ transition of tryptophan in the KWGK complex of poly(U). Excitation was at 297 nm using 16 nm bandwidth; the emission was monitored at 413.2 nm with 3.2 nm bandwidth. The microwave frequency, started at 1.4 GHz, was swept at (a) 80 and (b) 40 MHz/s with $t_0 = 5$ s. Superimposed solid lines represent the best fit of each response based on parameters given in Table 1.

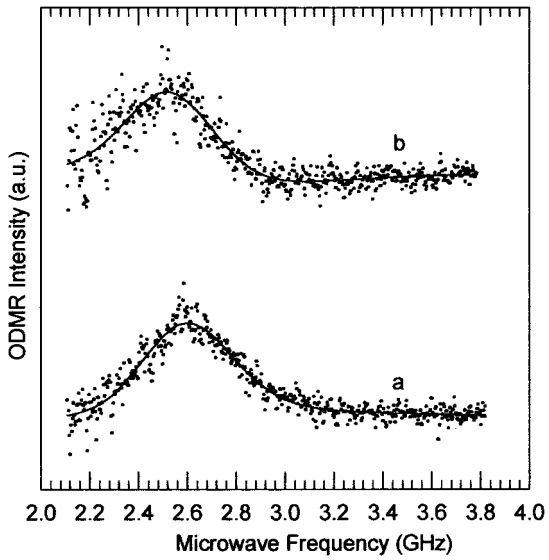

FIGURE 5: Delayed slow-passage ODMR spectra of the $2E$ transition of tryptophan in the KWGK complex of poly(U). Excitation was at 297 nm using 16 nm bandwidth; the emission was monitored at 413.2 nm with 3.2 nm bandwidth. The microwave frequency, started at 2.2 GHz, was swept at (a) 80 and (b) 40 MHz/s with $t_0 = 5$ s. Superimposed solid lines represent the best fit of each response based on parameters given in Table 1.

transition of the same complex are shown in Figure 5. The superimposed calculated responses are based on least-squares fittings, as with the $D-E$ transition. The results for the tryptophan peptides and their complexes are collected in Table 1; those for the 6-methyltryptophan peptides and their complexes are in Table 2. With the exception of the poly(A) complexes, each delayed slow-passage analysis was carried out using the kinetic and radiative rate constants obtained from the corresponding MIDP analysis as input parameters (*43*). Because of interference with poly(A) emission the slow passage ODMR bands of poly(A) complexes were analyzed by the previous method (*42*) that employs empirical kinetic parameters. Although only one example of a delayed slow passage spectrum is given for each sample in Figures 4 and 5, each experiment was repeated typically 4 or 5 times using different microwave sweep rates and sweep delay times. The values of ν_0 and $\nu_{1/2}$ given in Tables 1 and 2 are mean values from separate analysis of each data set. The standard deviations are determined largely by the variance in these analyses. The delayed ODMR signal in the $D-E$ band of the poly(A) complexes appeared as a partially resolved doublet due to the presence of adenine triplet states. These signals were analyzed as described previously (*32*). In the poly(A) complexes, the $2E$ bands ($T_x \leftrightarrow T_y$ transition) of adenine also overlap with those of the peptides, but doublets are not resolved; data were used only for long delay times to allow the shorter-lived T_y sublevel of adenine (relative to T_y of the peptides) to decay.

DISCUSSION

Phosphorescence and ODMR. Interaction of the tetrapeptides with polynucleotides and rG_8 is accompanied by red shifts of the phosphorescence 0,0-band and reduction of the ZFS D value. Similar effects of binding to these substrates have been observed from Trp37 of NCp7. The 0,0-band energies and ODMR frequencies of KWGK and KGWK differ slightly (Table 1), indicating some differences in local environment. They both differ from NCp7 [$\lambda_{0,0} = 409.6$ nm, $D = 2.972$ GHz (*32*)], although those of KGWK are closer.

Increased polarizability of the environment leads not only to a phosphorescence red-shift but also to a decrease in ZFS.

This indicates that the triplet state electron distribution becomes more diffuse in an increasingly polarizable environment resulting in a decrease of the magnetic dipole−dipole interaction that controls the ZFS. Further, the extent of solvent-induced red-shift and ZFS shifts are theoretically predicted, as well as found experimentally, to be linearly correlated with a positive dimensionless slope $(\Delta D/\Delta E_{0,0})$ on the order of $10^{-6}-10^{-5}$ (*36*−*38*). The theoretical model invokes solvent−molecule interactions that perturb the phosphorescent state, resulting in an admixture of more highly excited triplet states that are localized on the molecule. Both a lowering of the phosphorescent state energy and a reduction of ZFS result, since the higher energy admixed triplet states generally are expected to be more diffuse than the phosphorescent state. A slope of $\Delta D/\Delta E_{0,0} = 3.7 \times 10^{-6}$ is exhibited by tryptophan in 50% (v/v) ethylene glycol−water glass when using narrow band optical selection within the 0,0-band (*47*). We have made similar measurements on 6-methyltryptophan (data not shown) and have obtained a slope of $\Delta D/\Delta E_{0,0} = 3.1 \times 10^{-6}$, very similar to that of tryptophan. In previous work (*32*), we have argued that values of $\Delta D/\Delta E_{0,0}$ in excess of that exhibited by tryptophan in nonaromatic solvents results from the admixture of charge-transfer (CT) character into the phosphorescent state as a consequence of aromatic stacking interactions. CT states will reduce the ZFS to a far greater extent than a comparable admixture of localized triplet states because the electron dipole−dipole interaction, eqs 1 and 2, is effectively intermolecular in the former. The extent of mixing of the CT triplet state, $^3\Psi_{CT}$, with the phosphorescent state, $^3\Psi_1$, will depend inversely on the energy splitting, ΔE_{CT}, which can be estimated for nucleic acid N as,

$$E(^3\Psi_{CT}) - E(^3\Psi_1) \equiv \Delta E_{CT} \approx \mathrm{IP(Trp)} - E_{0,0}(\mathrm{Trp}) - \mathrm{EA(N)} + C \quad (6)$$

where IP and EA are the vertical ionization energy and electron affinity and C consists of the Coulomb and polarization energy of the ion pair (*48*). Vertical gas phase EA values for the common bases have been calculated recently using ab initio molecular orbital methods (*49*). The vertical EAs of the bases are found to increase in the order G < A < C < T < U, with values of −1.23, −0.74, −0.40, −0.32, and −0.19 eV, respectively. The EA of hypoxanthine was not calculated. The adiabatic EA of G and A are predicted to be negative as well, suggesting that G and A anions are unstable with respect to ionization in the vapor phase. The vertical IP of skatole has been measured to be 7.54 eV (*50*), which can be used for tryptophan. A reasonable estimate for C is −3.0 eV, and $E_{0,0} = 3.0$ eV. Using these values in eq 6, we estimate that ΔE_{CT} lies between 1.7 eV for U and 2.8 eV for G complexes.

We have plotted ΔD vs $\Delta E_{0,0}$ for each of the tryptophan-containing (Figure 6) and 6-methyltryptophan-containing (Figure 7) tetrapeptide complexes with nucleic acids. The straight lines in Figures 6 and 7 represent slopes of 3.7×10^{-6} and 3.1×10^{-6}, respectively, which are exhibited by tryptophan and 6-methyltryptophan in 50% (v/v) ethylene glycol−water glass where the solvent shifts do not involve aromatic stacking interactions. The slopes are obtained experimentally by measuring ODMR with narrow band detection through the inhomogeneously broadened 0,0-band.

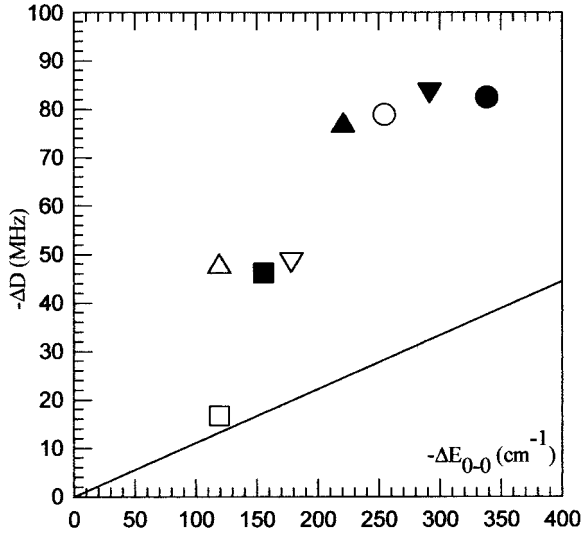

FIGURE 6: Plot of zfs shift $(-\Delta D)$ vs the phosphorescence red shift $(-\Delta E_{0,0})$ for KWGK and KGWK complexes of the nucleic acids: (■, □) KWGK, KGWK with rG_8; (▲, △) KWGK, KGWK with poly(A); (▼, ▽) KWGK, KGWK with poly(I); (●, ○) KWGK, KGWK with poly(U). The straight line represents $\Delta D/\Delta E_{0,0} = 3.7 \times 10^{-6}$, the slope exhibited by tryptophan in aqueous ethylene glycol glass.

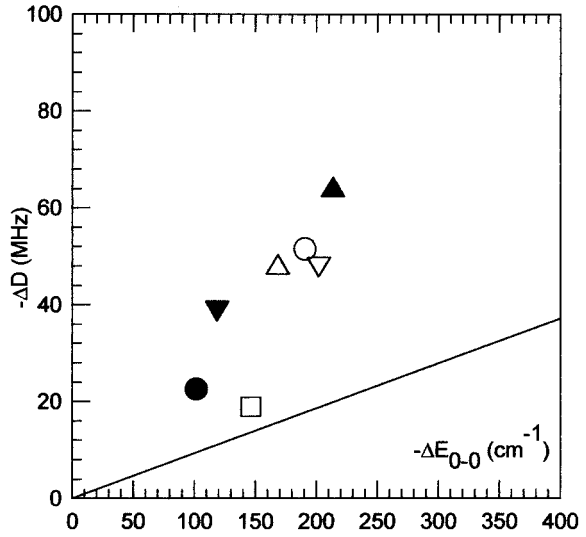

FIGURE 7: Plot of zfs shift $(-\Delta D)$ vs the phosphorescence red shift $(-\Delta E_{0,0})$ for K(6MeW)GK and KG(6MeW)K complexes of the nucleic acids: (■, □) K(6MeW)GK, KG(6MeW)K with rG_8; (▲, △) K(6MeW)GK, KG(6MeW)K with poly(A); (▼, ▽) K(6MeW)-GK, KG(6MeW)K with poly(I); (●, ○) K(6MeW)GK, KG-(6MeW)K with poly(U). The straight line represents $\Delta D/\Delta E_{0,0} = 3.1 \times 10^{-6}$, the slope exhibited by 6-methyltryptophan in aqueous ethylene glycol glass.

It is clear from both Figures 6 and 7 that most of the data points lie above the straight line and thus have values of $\Delta D/\Delta E_{0,0}$ in excess of the aliphatic solvent-induced shift. Values of $\Delta D/\Delta E_{0,0}$ for the complexes investigated in this work are given in Table 1 for tryptophan and in Table 2 for 6-methyltryptophan.

The observed shifts of $E_{0,0}$ are associated, in general, with mixing of both localized and CT triplet states. In a recent paper (*51*), we proposed that the maximum value for $\Delta D/\Delta E_{0,0}$ would occur if a stacking-induced interaction was limited to the admixture of a single CT triplet state. Neglecting electron overlap between the donor and acceptor pair and assuming that the singlet and triplet CT states are

effectively degenerate because the exchange energy should be small, it was shown that the value of $(\Delta D/\Delta E_{0,0})_{max}$ is given approximately by

$$(\Delta D/\Delta E_{0,0})_{max} \approx D^{(0)}(1/\Delta E_{CT} + 1/E_{0,0}) \qquad (7)$$

where $D^{(0)}$ is the unperturbed ZFS parameter. It should be noted that according to this model an analogous expression is anticipated for the ZFS parameter E. E, however, appears to be very sensitive to small admixtures of localized triplet states (*32*).

For tryptophan, using ΔE_{CT} estimated from eq 6, $D^{(0)} = 9.8 \times 10^{-2}$ cm^{-1}, and $E_{0,0} = 2.5 \times 10^4$ cm^{-1}, we find $(\Delta D/\Delta E_{0,0})_{max} \approx 11 \times 10^{-6}$ for U, $\approx 9 \times 10^{-6}$ for A, and $\approx 8 \times 10^{-6}$ for G. These estimates are quite similar, and considering the approximations leading to eq 7, the differences may not be significant. Probably all that can be concluded is that measured values of $\Delta D/\Delta E_{0,0}$ approximating 10^{-5} are indicative of significant CT character induced by transannular π-electron interactions. Values near 3.7×10^{-6} indicate localized triplet state admixture and the absence of significant stacking effects. Differences between stacking effects induced by different bases would assume greater significance for more effective π-electron donors than tryptophan, in which case ΔE_{CT} would be smaller for each base and differences in their EA would come into greater play. There is no appropriate experimental value of the IP for 6-methyltryptophan to provide an estimate of $(\Delta D/\Delta E_{0,0})_{max}$ for its nucleic acid interactions. On the basis of comparing measured values of IP between 1-methylnaphthalene and various dimethylnaphthalene isomers (*50*), methylation would not be expected to change the IP of skatole significantly. Therefore, $(\Delta D/\Delta E_{0,0})_{max}$ of 6-methyltryptophan complexes would probably be similar to those of tryptophan.

Since solvent−solute interactions are expected to admix localized triplet states along with the CT state if stacking interactions are present, we expect that nucleic acid binding will lead generally to values of $\Delta D/\Delta E_{0,0}$ that are less than the maximum values estimated above. The measured values of $(\Delta D/\Delta E_{0,0})$ (Table 1) for the tryptophan-containing complexes with poly(U), poly(A), and rG_8 are near 10^{-5}, except for the KGWK-rG_8 complex, which is substantially less. This agreement with the estimated values of $(\Delta D/\Delta E_{0,0})_{max}$ suggests that the introduction of CT character via transannular π-electron interactions plays a dominant role in the former complexes. Charge transfer in rG_8 complexes is smaller for KGWK than for KWGK. The EA of hypoxanthine is probably not too different than that of G or A, so values of ca. 10^{-5} observed for poly(I) complexes of KGWK and KWGK (Table 1) suggest considerable stacking-induced CT.

The data for the 6-methyltryptophan tetrapeptides (Table 2) parallel those of the corresponding tryptophan analogues. The observed values of $\Delta D/\Delta E_{0,0}$ fall in the same range. The K(6MeW)GK-rG_8 complex has an exceptionally large reduction of D, indicating significant CT, but $\Delta E_{0,0}$ could not be determined because of the intense G phosphorescence background (Figure 2). There is a definite sequence dependence of the peptide interaction with rG_8, KGXK showing less CT than KXGK (X = tryptophan, 6-methyltryptophan). It is interesting that NCp7, whose Trp37 sequence resembles KGWK more closely, reveals (*32*) minimal CT interactions with rG_8 ($\Delta D/\Delta E_{0,0} = 2.0 \times 10^{-6}$). NCp7, on the other hand, reveals considerable stacking with poly(U) and poly(I) yielding $\Delta D/\Delta E_{0,0} = 12 \times 10^{-6}$ and 8.1×10^{-6}, respectively. These are comparable to the values observed for the corresponding KGWK complexes. Then again, NCp7 produces very small red-shifts and ZFS shifts when combined with poly(A), in contrast with all of the tetrapeptides.

Triplet State Kinetics. Although the MIDP measurements give no information about the effect of nucleic acid binding on the absolute sublevel populating rates, it can be seen from the data in Tables 3 and 4 that the pattern of relative populating rates is affected significantly in some cases by complex formation. The p_x/p_y ratio barely changes over the series of complexes, except for the poly(U) complexes, where a small increase occurs. The relative value of p_z increases significantly in each poly(C) complex and to a lesser extent in the rG_8 complexes. Intersystem crossing from the excited singlet state is known to populate the T_x and T_y sublevels of the $^3(\pi,\pi^*)$ phosphorescent state of planar aromatic molecules selectively (*52*). Interaction with nucleobases does not enhance the relative value of p_z (*32*, *46*). Therefore, we suspect that the large value of p_z found in the poly(C) and rG_8 complexes results from triplet−triplet energy transfer from the cytosine and guanine bases. The background phosphorescence from the nucleic acids is particularly strong in these complexes. This mechanism would be expected to populate the sublevels less selectively than ISC, since it depends on the projection of donor principal magnetic axes on those of the acceptor (*53*), which should be quite random in these complexes. The value of k_z remains near zero in the poly(C) and rG_8 complexes confirming that the large relative p_z does not result from sublevel-selective SOC enhancement.

The value of k_x exhibits only minor changes in the tetrapeptide complexes. Far larger effects of nucleic acid binding are found (*32*, *46*) for Trp37 in NCp7. Increases in k_x and p_x/p_y of NCp7 are a great deal larger for a given substrate. When NCp7 forms a complex with poly(I), for example, k_x increases from 0.33 to ≥ 0.5 s^{-1}, while p_x/p_y increases from 0.84 to 3.05. The ISC pathways and rate constants as well as the radiative decay rate constants of triplet states are controlled by internal SOC, particularly by its effect of mixing singlet state character into triplet sublevels (*35*, *54*). Symmetry plays an important role in this pattern; it is noteworthy that it is k_x as well as p_x of Trp37 in NCp7 that are selectively enhanced by nucleic acid binding (*32*). It is found for both NCp7 and the tetrapeptides that $k_z \sim 0$. This observation is readily understood from the fact that the z-component of the SOC operator is extremely small in $^3(\pi,\pi^*)$ states of aromatic molecules (*55*, *56*). It has been noted that formation of CT complexes between aromatic molecules containing only light atoms leads to enhanced ISC in the triplet state of the donor and to reduced triplet state lifetimes (*57*, *58*); both are consistent with the enhancement of SOC-induced mixing between triplet and singlet states. Enhancement of ISC of proflavin when it is bound to DNA has been observed by Lee and Galley (*59*), but no change in triplet state lifetime was reported. In both the tetrapeptides and NCp7, we find CT contributions to the triplet state, but only in the case of NCp7 do we also find increased ISC. We propose that these differences may be the result of differing modes of tryptophan−base interaction, which we will now discuss.

Intercalation, Stacking, and Edge-On Interaction. The results presented in the previous sections may provide clues to the structural arrangement that is adopted by tryptophan or its analogue in the nucleic acid complexes. Tryptophan interactions with the nucleobases can be thought of in terms of three limiting arrangements, each of which can help to stabilize a protein−nucleic acid complex: (i) intercalation, in which the tryptophan is inserted between two bases in a stacked configuration allowing π-orbitals to interact; (ii) stacking, in which a *single* base interacts with tryptophan, again in a stacked configuration that allows for π-orbital interactions; and (iii) edge-on arrangement, in which the base approaches tryptophan at right angles minimizing π-electron interactions and with its positively charged edge imbedded in the π-electron cloud. These arrangements are expected to lead to different effects on the triplet state. As suggested some time ago by El-Sayed, et al. (*52*), enhancement of SOC can result from *static distortions that effectively remove the symmetry plane of an aromatic molecule*, allowing for the mixing of σ and π orbitals. Such distortions selectively enhance SOC in the in-plane sublevels (T_x and T_y in our coordinate system). From this point of view, we can distinguish between intercalation and the other two arrangements since the former is inherently more *symmetric* relative to the tryptophan plane than the latter. Stacking and edge-on arrangements, being inherently more *unsymmetric*, should result in greater enhancement of SOC. On the other hand, both intercalation and stacking, in contrast with an edge-on interaction are characterized by transannular π-orbital overlap that leads to a phosphorescence red shift and induced CT character, as described earlier. Edge-on interaction should produce a red shift, but induce no CT character, an arrangement thus characterized by small $\Delta D/\Delta E_{0,0}$.

The most striking difference between the tetrapeptide complexes and those of NCp7 is the greater enhancement of SOC in the latter. On the basis of the discussion above, we suggest that in the tetrapeptide complexes the aromatic amino acid is intercalated between bases, while in the NCp7 complexes tryptophan interacts most strongly with a single base in either a stacking or edge-on arrangement. Intermediate arrangements with varying degrees of π-orbital overlap are likely to occur, of course, but these will have a range of CT character and varying values of $\Delta D/\Delta E_{0,0}$. With two exceptions, the rG_8 complexes of KGWK and KG(6MeW)K, each of the tetrapeptide complexes exhibits a large value of $\Delta D/\Delta E_{0,0}$ consistent with CT character induced by transannular π-orbital overlap. Since the aromatic residue of the unstructured tetrapeptide has much more configurational freedom than Trp37 of NCp7, it would have greater freedom to intercalate between bases, while intercalation of Trp37 of NCp7 may not be possible because of steric constraints imposed by the zinc finger structure.

Enhancement of ISC in tryptophan that interacts with nucleic acids could be an effective contributor to fluorescence quenching that is in wide use to monitor protein−nucleic acid interactions. This mechanism has been suggested previously (*59*) to account for quenching of proflavin fluorescence when it binds to DNA.

CONCLUSIONS

The pattern of ZFS changes and phosphorescence red-shifts of tryptophan and 6-methyltryptophan in the tetrapeptide complexes are consistent with the presence of aromatic stacking interactions, similar to those reported earlier for NCp7 complexes (*32*). Values of $\Delta D/\Delta E_{0,0}$ are consistent with considerable induced CT character resulting from transannular π-orbital interactions between the aromatic amino acid and the nucleobases in most of the complexes. The smallest degree of CT character occurred in the rG_8 complexes of KGWK and KG(6MeW)K, in contrast with the alternate sequences, KWGK and K(6MeW)GK, which reveal significant CT involvement. Thus, the interaction with rG_8 varies significantly with the sequence of the peptide.

The triplet state kinetics of the tetrapeptides change very little in the nucleic acid complexes in contrast with NCp7 complexes in which significant enhancement of rates are found. These differences are attributed to differing arrangements of the aromatic amino acid relative to the nucleobases in the complex. They are consistent with *intercalation* of the amino acid between a pair of bases in the tetrapeptide complexes, but with less symmetrical *stacking* or *edge-on* arrangement with a single base in the NCp7 complexes. The enhancement of ISC and decay rates in the NCp7 complexes reflects the increase of SOC induced by elimination of the planar symmetry of the aromatic amino acid by an unsymmetrical interaction with a base (*52*). The differences in nucleic acid binding modes is attributed to steric constraints imposed on Trp37 of NCp7 by the local zinc finger structure that are not present in the tetrapeptides.

REFERENCES

1. Yarus, M. (1969) *Annu. Rev. Biochem. 38*, 841.
2. Hwang, P. C. (1971) *Prog. Biophys. Mol. Biol. 23*, 103.
3. Montenay-Garestier, T., and Hélène, C. (1968) *Nature* (*London*) *223*, 1061.
4. Montenay-Garestier, T., and Hélène, C. (1971) *Biochemistry 10*, 300.
5. Hui Bon Hoa, G., and Douzou, P. (1971) *J. Chim. Phys. Suppl.* 197.
6. Wagner, T. E. (1969) *Nature* (*London*) *222*, 1170.
7. Smythies, J. R., and Antun, F. (1969) *Nature* (*London*) *223*, 1061.
8. Hélène, C. (1971) *Nature* (*London*), *New Biol. 234*, 120.
9. Raszka, M., and Mandel, M. (1971) *Proc. Natl. Acad. Sci. U.S.A. 86*, 1190.
10. Brun, F., Toulmé, J. J., and Hélène, C. (1975) *Biochemistry 14*, 558.
11. Hélène, C., Brun, F., and Yaniv, M. (1969) *Biochem. Biophys. Res. Commun. 37*, 393.
12. Farrelly, J. G., Longworth, J. W., and Stulberg, M. P. (1971) *J. Biol. Chem. 246*, 1266.
13. Hélène, C. (1971) *FEBS Lett. 17*, 73.
14. Hélène, C., Toulmé, F., Charlier, M., and Yaniv, M. (1976) *Biochem. Biophys. Res. Commun. 71*, 3429.
15. Durand, M., Maurizot, J.-C., Borazan, H. N., and Hélène, C. (1975) *Biochemistry 14*, 563.
16. Gabby, E. J., Sanford, K., and Baxter, C. S. (1972) *Biochemistry 11*, 3429.
17. Hélène, C., and Dimicoli, J.-L. (1972) *FEBS Lett. 26*, 6.
18. Dimicoli, J.-L., and Hélène, C. (1974) *Biochemistry 13*, 714, 724.
19. Co, T.-T., and Maki, A. H. (1978) *Biochemistry 17*, 182.
20. Maki, A. H., and Cha, T.-A. (1984) in *Photochemistry and Photobiology* (Zewail, A., Ed.) Vol. 2, p 1035, Harwood Academic Press, Chur, Switzerland.
21. Khamis, M. A., Casas-Finet, J. R., and Maki, A. H. (1987) *J. Biol. Chem. 262*, 1725.
22. Zang, L. H., Maki, A. H., Murphy, J. B., and Chase, J. W. (1987) *Biophys. J. 52*, 867.

23. Tsao, D. H. H., Casas-Finet, J. R., Maki, A. H., and Chase, J. W. (1989) *Biophys. J. 55*, 927.
24. Lam, W.-C., Maki, A. H., Casas-Finet, J. R., Erickson, J. W., Sowder, R. C., II, and Henderson, L. E. (1993) *FEBS Lett. 328*, 45.
25. Wu, J. Q., Maki, A. H., Ozarowski, A., Urbaneja, M. A., Henderson, L. E., and Casas-Finet, J. R. (1997) *Biochemistry 36*, 6115.
26. Mascotti, P. D., and Lohman, M. T. (1997) *Biochemistry 36*, 7272.
27. Mascotti, P. D., and Lohman, M. T. (1992) *Biochemistry 31*, 8932.
28. Zuclich, J., von Schütz, J. U., and Maki, A. H. (1974) *J. Am. Chem. Soc. 96*, 710.
29. Ghosh, S., Zang, L.-H., and Maki, A. H. (1988) *Biochemistry 27*, 7816.
30. Ozarowski, A., Barry, J. K., Matthews, K. S., and Maki, A. H. (1999) *Biochemistry 38*, 6715.
31. Lam, W. C., Maki, A. H., Casas-Finet, J. R., Erickson, J. W., Kane, B. P., Sowder, R. C., II, and Henderson, L. E. (1994) *Biochemistry 33*, 10693.
32. Wu, J. Q., Ozarowski, A., Maki, A. H., Urbaneja, M. A., Henderson, L. E., and Casas-Finet, J. R. (1997) *Biochemistry 36*, 12506.
33. Goerlick, R. J., Henderson, L. E., Hanser, J. P., and Rein, A. (1988) *Proc. Natl. Acad. Sci. U.S.A. 85*, 8420.
34. Méric, C., and Goff, S. P. (1989) *J. Virol. 63*, 1558.
35. McGlynn. S. P., Azumi, T., and Kinoshita, M. (1969) *Molecular Spectroscopy of the Triplet State*, Prentice-Hall, Englewood Cliffs, NJ.
36. van Egmond, J., Kohler, B. E., and Chan, I. Y. (1975) *Chem. Phys. Lett. 34*, 423.
37. Gradl, G., Friedrich, J., and Kohler, B. E. (1986) *J. Chem. Phys. 84*, 2079.
38. Williamson, R. L., and Kwiram, A. L. (1988) *J. Chem. Phys. 88*, 6092.
39. Haenel, M. W., and Schweitzer, D. (1988) *Adv. Chem. Ser. 217*, 333.
40. Ozarowski, A., Wu, J. Q., and Maki, A. H. (1996) *J. Magn. Reson. Ser. A 121*, 178.
41. Wu, J. Q., Ozarowski, A., and Maki, A. H. (1996) *J. Magn. Reson. Ser. A 119*, 82.
42. Wu, J. Q., Ozarowski, A., Davis, S. K., and Maki, A. H. (1996) *J. Phys. Chem. 100*, 11496.
43. Ozarowski, A., and Maki, A. H. (2000) *J. Phys. Chem. B 104*, 1122.
44. Ozarowski, A., Wu, J. Q., and Maki, A. H. (1998) *FEBS Lett. 422*, 52.
45. Purkey, R. M., and Galley, W. C. (1970) *Biochemistry 9*, 3569.
46. Ozarowski, A., and Maki, A. H., unpublished work.
47. Von Schütz, J. U., Zuclich, J., and Maki, A. H. (1974) *J. Am. Chem. Soc. 96*, 714.
48. Mulliken, R. S. (1952) *J. Am. Chem. Soc. 74*, 811.
49. Sevilla, M. D., Besler, B., and Colson, A.-O. (1995) *J. Phys. Chem. 99*, 1060.
50. Lias, S. G., Barmess, J. E., Liebman, J. F., Holmes, J. L., Levin, R. D., and Mallard, W. G. (1988) *J. Phys. Chem. Ref. Data 17*, *Suppl. 1*.
51. Maki, A. H., Ozarowski, A., Misra, A. K., Urbaneja, M. A., and Casas-Finet, J. R., submitted for publication.
52. El-Sayed, M. A., Moomaw, W. R., and Chodak, J. B. (1973) *Chem. Phys. Lett. 20*, 11.
53. El-Sayed, M. A., Tinti, D. S., and Yee, E. M. (1969) *J. Chem. Phys. 51*, 5721.
54. van der Waals, J. H., and de Groot, M. S. (1967) in *The Triplet State* (Zahlan, A. B., Ed.) p 101, Cambridge University Press, Cambridge.
55. Weissman, S. I. (1950) *J. Chem. Phys. 18*, 232.
56. McClure, D. S. (1952) *J. Chem. Phys. 20*, 682.
57. Czekalla, J., Briegleb, G., Herre, W., and Vahlensieck, H. J. (1959) *Z. Elektrochem. 63*, 715.
58. Christodouleas, N., and McGlynn, S. P. (1964) *J. Chem. Phys. 40*, 166.
59. Lee, W. E., and Galley, W. C. (1988) *Biophys. J. 54*, 627.

BI0015663